INTERNATIONAL JOURNAL FOR NUMERICAL METHODS IN FLUIDS, VOL. 5, 849–871 (1985)

A RANDOM VORTEX SIMULATION OF WIND-FLOW OVER A BUILDING

D. M. SUMMERS, T. HANSON AND C. B. WILSON

Department of Architecture, University of Edinburgh, 20 Chambers Street, Edinburgh EH1 1JZ, Scotland

SUMMARY

The random vortex method of Chorin[1] provides a numerical simulation of high-Reynolds number flow in two dimensions. The method can be used to model the viscous interaction of wind with a surface-mounted obstacle of arbitrary cross-section. In this paper the method has been used to investigate the flow of wind over common building shapes; an inlet profile is chosen to represent the stationary aspects of the atmospheric boundary layer. The evolution of flow over a short time-interval after flow initialization is depicted, and a mean value of pressure coefficient, C_p, is calculated over the building perimeter. Some comparison is made with published wind-tunnel measurements for the case of a surface-mounted square-section block and for a building model with 10° roof pitch.

KEY WORDS Random Vortex Method Wind Engineering

1. INTRODUCTION

Any mathematical expression which describes the complete physical problem of a slightly viscous fluid flowing over a bluff obstacle leads to considerable complexity. The governing Navier–Stokes equation is, of course, non-linear and it is precisely the non-linear character of the general solutions to this equation which is of importance in the study of aerodynamics for bluff bodies. Moreover, the difficulties of effecting numerical solutions to the equation are well-known. In the particular case of wind flowing around buildings, these inherent mathematical and numerical difficulties are further complicated by the nature of environmental boundary conditions.

As a result of these complexities, little attempt has been made to bring solutions of the Navier–Stokes equation to bear on the problem of wind-induced structural loading. Our physical understanding derives in large part from controlled scale-model experiments in wind-tunnels, together with full-scale pressure measurements on buildings. Theoretical discussion has been confined usually to first-order linearizations and to dimensional analysis.

Vortex shedding from a bluff obstacle such as a building (and the consequent formation of a wake) is a complicated phenomenon which is still the subject of experimental investigation, e.g. see References 2–4. Over recent years considerable progress has been made towards finding numerical solutions to the Navier–Stokes equation and it may be asked whether these can contribute to an understanding of the physical processes. Concerning the specific problem of the wind-loading of structures, there are a number of questions which experiment has not yet fully resolved.

1.1. Scaling assumptions

The use of reduced-scale models of buildings in an unpressurized wind-tunnel can imply a

0271–2091/85/100849–23$02.30 *Received March 1985*

reduction in Reynolds number of as much as three orders of magnitude from the corresponding full-scale case.

For buildings with sharp edges, the statement is often made that vortex shedding from sharp corners (coinciding with the location of fixed separation points) is largely independent of Reynolds number. The Strouhal number in such cases is observed to show little dependence on Reynolds number (e.g. see Figure 2 in Reference 5). Such observations offer some reassurance that the spanwise vortex shedding from the leeward vertical walls of a rectangular building (if it is sufficiently tall) can be confidently modelled in a wind-tunnel. However, flow separating from a curved surface exhibits dependence on Reynolds number and in recent years this knowledge has inhibited the use of wind-tunnels for the study of wind-loading requirements for buildings with curved surfaces.

The streamwise shedding of vorticity from the top of a two-dimensional surface-mounted obstacle exhibits a much broader frequency spectrum than that associated with spanwise shedding and a vortex street.[6] It is not clear whether a flow such as this—with periodicity which is much less sharply-defined—will be independent of Reynolds number. The results reported in Reference 7 suggest that there is some dependence on Reynolds number for flow over prismatic hill-models. The question is worth pursuing since, from the point of view of understanding the dynamical aspects of wind-loading on pitched roofs, this streamwise mode is of particular interest.

1.2. Turbulence

Perhaps the most significant complicating factor affecting the study of wind-loading is the unsteady and turbulent nature of the wind-flow to which buildings are subjected. Recent research has been devoted to determining a mathematical description for the turbulence of strong winds.[8] The efficacy of the wind-tunnel as a design and research tool relies to some extent upon an adequate simulation of natural wind turbulence, appropriately scaled. (The scaling of turbulence has also been investigated, for example in Reference 9.)

In general, a distribution of turbulence intensity determined for an established wind-profile in open country cannot describe the wind exposure of urban buildings. Indeed, how confidently any universal power-law boundary-layer profile (with an associated turbulence intensity) can be used to study wind-loading in a densely built environment is a matter for some conjecture. Even in cases of isolated buildings in open country, the discrepancy between full-scale field measurements and predictions derived from wind-tunnel measurements has, on occasion, been attributed to the difficulties of representing natural wind turbulence in a wind-tunnel.[10]

1.3. Estimating mean flow

The mean flow parameters deduced from wind measurements depend upon the time-interval over which such averages are calculated. A significant part of the wind-loading of buildings can be associated with the transient components of the wind. Gusts can have periods ranging from ten seconds down to tenths of a second, and these latter, almost 'impulsive', fluctuations may give rise to local suction pressures many times greater than the pressure averages computed over longer time intervals.[11] High frequency fluctuations occur even when the incident wind is steady (in this case, the vorticity is generated by the viscous interaction of the wind with the building itself). To understand the wind-induced local stresses to which surface cladding is subjected, it is necessary to understand the mechanism of this viscous interaction, and to appreciate how mean pressure estimates are affected by their time-interval of averaging.

Particular difficulties arise when such high frequency phenomena are studied in a wind-tunnel: typically the scaling of time for impulsive phenomena would require model measurements of pressure to be made at time intervals of less than 0.001 s.

2. THE RANDOM VORTEX METHOD

We suggest that the interaction of a building with its wind-flow field can be studied by directly solving the Navier–Stokes equation. For numerical solutions to have a bearing on the wind-loading problems which we have discussed, the solution procedure should ideally have the following characteristics: (i) it should be as free as possible from 'artificial viscosity' error—the errors implicit to the numerical approximation should be independent of Reynolds number; (ii) it should be able to solve for the case of a building interacting with a flow-field with a prescribed vorticity content, and hence be able to simulate the dynamical flow interaction of one building with another and with upstream turbulence; and (iii) it should be capable of solving for impulsive phenomena and of rendering the evolution of flow over short intervals of time. The random vortex method of Chorin[1,12,13] should be able to satisfy these requirements.

The flow dynamics of a slightly viscous fluid can be given a numerical description by the discretizing of its vorticity field into a distribution of localized vortices of small finite core size (called vortex 'elements' or 'blobs'). As far as the inviscid aspect of their motion is concerned, these vortices convect in the local velocity field of the fluid. Momentum diffusion is simulated by imparting to each vortex element a random-walk displacement and such a simulation can be accurate when taken in statistically significant aggregate.

We consider the flow of wind over a two-dimensional surface-mounted obstacle $\mathscr{A}$, with perimeter $\partial\mathscr{A}$, resting on the surface $y = 0$ in the (x, y)-plane. The problem is depicted in Figure 1.

There will be a viscous interaction between the obstacle and the inlet wind. We consider three flow regimes: far from the obstacle the flow is unperturbed and is represented mathematically by a

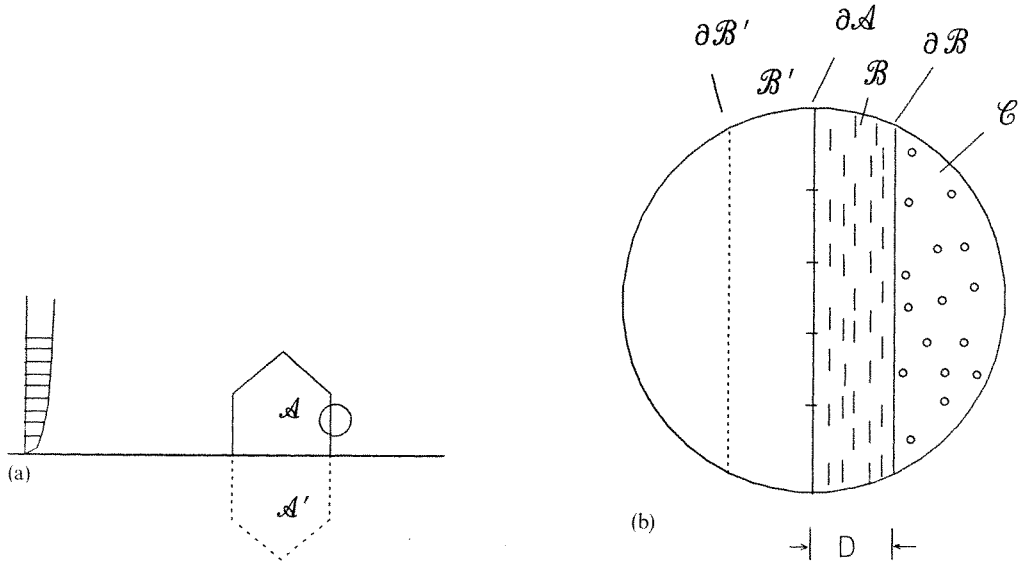

Figure 1(a). An obstacle in a sheared incident stream and (b) a microcosm of its boundary (— are sheet 'segments', ○ are vortex 'elements')

sheared free-stream profile; at $\partial\mathscr{A}$ itself a *boundary-layer*, $\mathscr{B}$, is formed in which the Prandtl boundary-layer approximation is assumed to be valid; beyond the envelope ($\partial\mathscr{B}$) of this boundary layer and in the downstream wake, the flow is complicated by the velocity field induced by vorticity which has been created by the interaction of the wind with the obstacle—this region is denoted as $\mathscr{C}$.

2.1. *The field in $\mathscr{C}$ induced by vorticity*

The incompressible dynamics of flow in region $\mathscr{C}$ is expressed through a scalar vorticity field, ξ. The curl of the Navier–Stokes equation can be expressed in dimensionless form,

$$\partial\xi/\partial t + \mathbf{u}\cdot\nabla\xi = Re^{-1}\nabla^2\xi, \tag{1}$$

with $\boldsymbol{\xi} = \operatorname{curl}\mathbf{u}$, and $\boldsymbol{\xi} = \xi\mathbf{k}$ for flow confined to $y > 0$ in the (x, y)-plane. The flow field $\mathbf{u}$ satisfies the continuity condition, so the flow field induced by vorticity ξ may be represented by a stream function ψ through

$$\nabla^2\psi = -\xi, \tag{2}$$

with $\mathbf{u} = (\partial\psi/\partial y, -\partial\psi/\partial x)$. The solution to (2) at a field point $\mathbf{r}_0$ is expressed in terms of its Green's function,

$$\psi(\mathbf{r}_0) = -\int \xi(\mathbf{r})G(\mathbf{r}_0|\mathbf{r})\,\mathrm{d}\mathbf{r}, \tag{3}$$

where $\mathbf{r} = x\mathbf{i} + y\mathbf{j}$, etc. The vorticity distribution $\xi(\mathbf{r})$ is discretized by considering a collection of point vortices located at positions $\{\mathbf{r}_j\}$, by

$$\xi(\mathbf{r}) = \sum_j \Gamma_j\delta(\mathbf{r} - \mathbf{r}_j), \tag{4}$$

where Γ_j is the circulation of the jth vortex element and δ is the Dirac delta-function. In fact, the Green's function appropriate to (3) is singular as $\mathbf{r}_0 \to \mathbf{r}$, so a modification is introduced to suppress this singularity. Rather than a point vortex, a vortex of small but finite core size, σ, is introduced (this being the source of a spatial truncation error in the simulation). The modified Green's function appropriate to a surface-mounted obstacle may be determined from image theory as

$$\mathbf{G}(\mathbf{r}_0|\mathbf{r}) = \begin{cases} (2\pi)^{-1}\{\log|\mathbf{r}_0 - \mathbf{r}| - \log|\mathbf{r}_0 - \mathbf{r}^*|\}, & |\mathbf{r}_0 - \mathbf{r}| \geqslant \sigma \\ (2\pi\sigma)^{-1}\{|\mathbf{r}_0 - \mathbf{r}| - |\mathbf{r}_0 - \mathbf{r}^*|\}, & |\mathbf{r}_0 - \mathbf{r}| < \sigma \end{cases} \tag{5}$$

($\mathbf{r}^*$ is the reflection of $\mathbf{r}$ across the ground plane $y = 0$). Thus when the field is computed at a position greater than a distance σ from a vortex element, the interaction is assumed to be the usual singular one between point vortices; when the field is computed within a radius σ of the vortex element we resort to a non-singular form for $G(\mathbf{r}_0|\mathbf{r})$. Substituting (5) and (4) into (3) provides a discretized expression for $\psi(\mathbf{r}_0)$ and hence an expression for the velocity field (u_ξ, v_ξ) induced by $\xi(\mathbf{r})$ at $\mathbf{r}_i$ can be determined as a numerical algorithm which consists of summations over the finite collection of discrete vortex elements. Cheer (Reference 14, p. 11), for example, provides a statement of this algorithm.

2.2. *Imposing the impermeability condition*

Two sources of vorticity are envisaged in the present problem: that entering the flow from upstream (see Section 2.5) and that generated by viscous interaction with the obstacle (see

Section 2.4). Once entered into inviscid flow, vorticity is transported in the local velocity field, with this transport described by the time-dependent Euler equation,

$$\partial\xi/\partial t + \mathbf{u}\cdot\nabla\xi = 0. \tag{6}$$

Numerically the convective displacement $\mathrm{d}\mathbf{x}_i$ in time $\mathrm{d}t$ of the ith vortex element we take to be the Euler step $\mathrm{d}\mathbf{x}_i = \mathbf{u}_i\,\mathrm{d}t$. During each time-interval of this evolution the condition of impermeability must be satisfied on $\partial\mathscr{A}$.

If $\mathbf{u}_\mathrm{f}$ represents the free-stream flow in the absence of the obstacle, and $\mathbf{u}_\xi$ represents the field induced at time t by the vorticity which has been generated at the obstacle in the previous time-steps, then we can construct an auxiliary velocity field $\mathbf{u}_\phi$ which is irrotational and which effects the condition

$$(\mathbf{u}_\mathrm{f} + \mathbf{u}_\xi + \mathbf{u}_\phi)\cdot\mathbf{n} = 0, \quad \text{on } \partial\mathscr{A}, \tag{7}$$

in the time interval $(t, t + \mathrm{d}t)$. Since the vorticity distribution is evolving in time, condition (7) must be re-established successively at each time interval. At any given time-step $\mathbf{u}_\phi$ is irrotational, i.e. it is Laplacian. When the boundary layer $\mathscr{B}$ is introduced, condition (7) will be imposed on $\partial\mathscr{B}$ rather than on $\partial\mathscr{A}$.

The procedure for constructing the field $\mathbf{u}_\phi$ (for an arbitrarily shaped two-dimensional obstacle) is described by Chorin[1] or Hanson *et al.*[15] This field can be represented by a scalar potential, ϕ, such that

$$\mathbf{u}_\phi = \nabla\phi, \tag{8}$$

which can be given a Green's function representation

$$\phi(\mathbf{r}_0) = \oint\gamma(\mathbf{r})G(\mathbf{r}_0|\mathbf{r})\,\mathrm{d}\mathbf{r} \tag{9}$$

Image theory is again invoked and this line-integration is taken over the extended perimeter of the obstacle together with its mirror image in $y < 0$, $\partial\mathscr{A} + \partial\mathscr{A}'$. To determine the unknown 'source-sink' distribution $\gamma(\mathbf{r})$, boundary condition (7) is applied, i.e. (9) is substituted into (8) and then (8) is substituted into (7). This leads to the integral equation

$$\gamma(\mathbf{r}_0) - \frac{1}{\pi}\oint\gamma(\mathbf{r})\frac{\partial}{\partial n}\{\log|\mathbf{r}_0 - \mathbf{r}|\}\,\mathrm{d}\mathbf{r} = -2(\mathbf{u}_\xi + \mathbf{u}_\mathrm{f})\cdot\mathbf{n}, \tag{10}$$

which is represented discretely as a system of linear equations. The values of γ evaluated at discrete points along the obstacle boundary are determined as the solution to

$$\mathbf{A}\boldsymbol{\gamma} = \mathbf{b}, \tag{11}$$

where $\mathbf{b}$ is the scalar array $2(\mathbf{u}_\xi + \mathbf{u}_\mathrm{f})\cdot\mathbf{n}$ evaluated at the discrete body points on $\partial\mathscr{A}$. The matrix $\mathbf{A}$ is a function only of the geometry of the obstacle: since it is functionally independent of the flow dynamics it requires to be inverted once only at the outset of computation. The elements of matrix $\mathbf{A}$ are given explicitly in Section 4 of Reference 1.

In the model describing the evolution of flow in terms of the convection of vortex elements, the effect of viscosity has not yet been taken into account. That is to say, the convective Euler's equation which results if the right-hand side of equation (1) is suppressed has been modelled. If instead, the convection term in this equation is suppressed—i.e. the term $\mathbf{u}\cdot\nabla\xi$—there results a diffusion equation, the solution of which (in the absence of boundaries) is an isotropic Gaussian distribution with zero mean and with standard deviation $(2\,\mathrm{d}t/Re)^{1/2}$. We follow Chorin[1,12] by exploiting the stochastic implications of such a process: after each time increment, $\mathrm{d}t$, to each

discrete vortex element a random Gaussian displacement, $\boldsymbol{\eta} = (\eta_x, \eta_y)$, is imparted which has zero mean and variance $2\,\mathrm{d}t/Re$. Taken in sufficiently large ensemble and over a period of time, addition of this discrete representation of diffusion to the field $\mathbf{u}_\xi + \mathbf{u}_\phi + \mathbf{u}_\mathrm{f}$ should simulate the entire flow of (1) in $\mathscr{C}$. The vector displacement $\mathrm{d}\mathbf{x} = (\mathrm{d}x_i, \mathrm{d}y_i)$ over a time interval $\mathrm{d}t$ of a discrete vortex element ξ_i can be expressed as

$$\mathrm{d}\mathbf{x}_i = \{\mathbf{u}_\xi(\mathbf{r}_i) + \mathbf{u}_\mathrm{f}(\mathbf{r}_i) + \mathbf{u}_\phi(\mathbf{r}_i)\}\,\mathrm{d}t + \boldsymbol{\eta}. \tag{12}$$

2.3. *Vorticity dynamics in* $\mathscr{B}$

The no-slip condition has not yet been imposed on the solution. It can be imagined that, as wind moves over the obstacle, a shear layer will form parallel to its surface. This will consist of vortex sheets (which are to be discretized into 'segments') of sufficient intensity and distribution that they effect a no-slip condition at the boundary. The vortex sheets generated in this way will form a boundary-layer. We consider such a layer of thickness D parallel to the surface of an arbitrarily-shaped two-dimensional obstacle. In this layer it is assumed that equation (1) can be approximated by the Prandtl boundary-layer equation

$$\partial\kappa/\partial t + \mathbf{u}_\kappa \cdot \nabla\kappa = \nu\partial^2\kappa/\partial y'^2 \tag{13}$$

with vorticity, $\kappa(x', y')$ in the boundary-layer, now given by

$$\kappa = -\partial u_\kappa/\partial y' \tag{14}$$

(ν is the kinematic viscosity of air; $\mathbf{u}_\kappa = (u_\kappa, v_\kappa)$ is the velocity field in $\mathscr{B}$). A local co-ordinate system (x', y') has been introduced such that x' is orientated parallel to $\partial\mathscr{A}$ and y' is orientated as an outward normal to it. A microcosm of this boundary is considered with local origin fixed at $\partial\mathscr{A}$ where $u_\kappa(x', y' = 0) = 0$. At $\partial\mathscr{B}$ the velocity $\mathbf{u}_\kappa$ must match that of the flow in $\mathscr{C}$ which has been previously discussed, i.e.

$$\mathbf{u}_\kappa(x', y' = D) = \mathbf{U}_D$$

with $\mathbf{U}_D(x') = \mathbf{u}_\xi(\mathbf{r}) + \mathbf{u}_\mathrm{f}(\mathbf{r}) + \mathbf{u}_\phi(\mathbf{r})$, where the global position in $\mathscr{C}$ indicated by $\mathbf{r}$ is understood to coincide with the local position relative to the boundary-layer $\mathscr{B}$ implied by $(x',\ y' = D)$. The potential field $\mathbf{u}_\phi$ is now to be calculated to ensure that there is no flow in the y'-direction across each point of $\partial\mathscr{B}$. The continuity condition in the boundary-layer,

$$\frac{\partial u_\kappa}{\partial x'} + \frac{\partial v_\kappa}{\partial y'} = 0,$$

is integrated so that

$$v_\kappa(x', y') = -\frac{\partial}{\partial x'}\int_0^{y'} u_\kappa(x', \lambda)\,\mathrm{d}\lambda \tag{15}$$

and equation (14) can be integrated in the form

$$u_\kappa(x', y') = U_D - \int_{y'}^{D} \kappa(x', \lambda)\,\mathrm{d}\lambda. \tag{16}$$

Chorin (Reference 12, p. 430) provides a discrete expression for (16) by considering the shear layer formed along $\partial\mathscr{A}$ to be discretized into vortex segments of intensities $\{\kappa_j\}$ and lengths $\{h_j\}$ orientated parallel to the boundary at body points $\{x'_j\}$. Collectively these will induce a motion on the ith segment denoted by $\mathbf{u}_\kappa = (u_\kappa, v_\kappa)$. If the vorticity in the boundary layer is determined by a

summation over discrete sheet segments, then the velocity field $\mathbf{u}_\kappa$ can be deduced from (15) and (16); hence the motion of a vortex segment in a time interval dt can be approximated by

$$\begin{aligned} dx_i' &= u_\kappa(x_i', y_i')\,dt, \\ dy_i' &= v_\kappa(x_i', y_i')\,dt + \eta', \end{aligned} \tag{17}$$

where η' represents a simulation of diffusion, i.e. it is a Gaussian random displacement with standard deviation $(2\nu dt)^{1/2}$. It is to be noted from equation (13) that boundary-layer diffusion proceeds only in the y'-direction.

2.4. *Imposing the no-slip condition: vortex creation*

If, after a time-step dt, the redistributed vorticity in $\mathscr{B}$ gives rise to a non-zero tangential velocity at $\partial\mathscr{A}$—i.e. if $u_\kappa(x', 0) = u_0 \neq 0$ when the $\{\kappa_j\}$ are substituted into (17)—then no-slip can be re-imposed by creating a vortex sheet with intensity (per unit length of the boundary) u_0. In itself, this would constitute a crude vorticity-creation algorithm.

Diffusion at a solid boundary is not an isotropic Gaussian process, so an algorithm assuming isotropy can be poorly convergent. A more appropriate vorticity-creation algorithm has been introduced by Chorin.[12] In order to construct a Gaussian diffusion which is isotropic at $y' = 0$ and which nevertheless allows all the required boundary conditions to be satisfied there, the flow field is formally 'extended' across the boundary such that $u_\kappa(x', -y') = -u_\kappa(x', y')$ and $u_\kappa(x', 0) = 0$. Such a field must imply that $\kappa(x', -y') = \kappa(x', y')$ for $y' \neq 0$. Thus, if after time interval dt there exists a non-zero tangential velocity u_0 at $(x', 0)$, a vortex sheet of intensity $2u_0$ is created there which is divided into $2l$ segments $\{\kappa_j\}$ and during the subsequent time-step these are made to diffuse isotropically into the extended boundary $-D < y' < +D$. The random displacement of the segments is made to proceed in alternate directions, so that half diffuse into $\mathscr{B}$, and half into the image layer, $\mathscr{B}'$ (these latter disappearing from the computation). Thus the introduction of the l segments into $\mathscr{B}$ impose with their collective intensity u_0 the no-slip condition at $\partial\mathscr{A}$. Further references related to the development of this algorithm are to be found in Reference 12.

The symmetry condition $\kappa(x', y') = \kappa(x', -y')$ implies that if a vortex segment moves into the image layer $\mathscr{B}'$, then it can be reflected back across $y' = 0$ into the boundary layer proper. By symmetry such a reflection procedure will, on average, simulate the diffusion across $y' = 0$ of vortex segments from the image layer $\mathscr{B}'$ into $\mathscr{B}$. If a sheet κ_i moves into the region $\mathscr{C}$, i.e. into $y' > +D$, then it becomes a discrete vortex element ξ_i such that $\xi_i = h_i\kappa_i$. Cheer[14] has shown that if a core size σ_i for this element is chosen so that $\sigma_i = h_i/\pi$ then the interaction of the sheet segment κ_i approximates that of the element ξ_i in the limit $y' \to D$. Alternatively if an element ξ_i enters the boundary layer from $\mathscr{C}$, it becomes a vortex sheet κ_i.

In view of the discrete vortex dynamics associated with such a model of the boundary layer, its thickness D should be a reasonable number of standard deviations in magnitude. In the examples to be presented in this paper, D is chosen to be five standard deviations in width.

2.5. *Upstream conditions*

It is our interest to study the interaction of a surface-mounted obstacle with an approach flow which models the atmospheric boundary layer. We approximate this by prescribing a logarithmic boundary layer profile at the inlet.

In principle a more complete simulation of this ambient flow can be attempted by 'growing' the boundary layer profile upstream through imposing the no-slip condition there. This would

simulate dynamically the vorticity in the approach flow. In order to generate a profile of prescribed structure, the numerical equivalent of roughness would need to be introduced upstream. Ideally such a model should also be made to represent the turbulence structure of wind. The task of constructing such an elaborate model of the atmospheric boundary layer is not pursued in the present paper, although it is within the scope of the random vortex method (see, for example, Reference 16).

The effect of upstream vorticity on the flow over an obstacle is of some considerable interest. Fraenkel[17] demonstrated analytically that in the case of vorticity incident on a surface-mounted obstacle, there develops a recirculation corner-flow to windward of the obstacle. Fraenkel considered the case of inviscid flow over an obstacle upon which free-slip conditions were imposed, in contrast to the present simulation in which Navier–Stokes flow is considered, with no-slip imposed at the obstacle.

The simplified numerical model presented here does not lend itself to investigating the effect of upstream vorticity on the flow. By representing the approach flow as a velocity profile, the incident vorticity does not participate itself in the evolving flow dynamics. After the first time-step the vorticity of the incident stream is assumed to be much less intense than that generated by no-slip at the obstacle; we consider that there is a considerable difference in scale between the atmospheric boundary-layer (some 400 m) and the thin boundary layer created by no-slip at the surface of the obstacle (some 2 cm). To adequately study the effect of varying the vorticity content of the approach flow, a more dynamically complete simulation of the atmospheric boundary layer would be required.

3. ACCURACY OF THE METHOD

The interaction of a slightly viscous fluid with a large bluff body is a numerically awkward problem when it is formulated as a difference analogue to the Navier–Stokes equation. If difference approximations of consistent order are made to the advection term in this equation (i.e. to $\mathbf{u}\cdot\nabla\mathbf{u}$) and to the viscous term (i.e. to $Re^{-1}\nabla^2\mathbf{u}$), the truncation error of the former can 'swamp' the entire viscous term, a hazard which obviously increases with increasing Reynolds number. The difference errors to the advection term have the structure of second-order spatial derivatives[18] and they can be considered to introduce a purely numerical diffusion into the difference method. The random vortex method is a useful alternative to difference methods because it circumvents this specific numerical 'swamping' effect. However, other kinds of numerical error are generated by the method.

3.1. Unbounded flow

Detailed error analysis has been applied to the vortex method for the case of flow in the absence of boundaries. The discretization of continuum vorticity into elements of finite core size, σ, generates a spatial truncation error; for inviscid flow, analyses of various vortex methods have determined this error to be of $O(\sigma^2)$.[19,20] Leonard also shows (for uniform core size) that this error is not diffusive to $O(\sigma^2)$; Marsden and Weinstein[21] demonstrate more generally that a collection of discrete vortices of fixed finite core size is a Hamiltonian system which therefore admits no dissipation.

Vortices of finite size should deform as they are convected. If this deformation is suppressed (as it obviously is in the present simulation) an error is introduced which is subsumed in the $O(\sigma^2)$ error of the vortex method.[19] Leonard[20] points out that the method is a Lagrangian treatment so no explicit treatment of the advective derivatives in (1) is required, and fairly large

time-steps can lead to stable solutions. It should be noted that Hald's[19] analysis includes a higher-order time-integration scheme of the Lagrangian co-ordinates, whereas in the present simulation the Euler solution is used. Temporal truncation should not contribute an error with diffusive structure.

The error associated with a Gaussian ensemble representation of diffusion in a static fluid is of order $\nu^{1/2}$. Beale and Majda[22] demonstrate that the vortex representation of Eulerian flow approximates viscous flow to $O(\sigma^2 + \nu)$ and they offer this as a lower bound to the composite error for inviscid flow plus a random-walk diffusion. Chorin[12] has estimated this composite error heuristically to be of $O(\sigma^2 + \nu^{1/2})$: in view of the result of Beale and Majda this may be a rather liberal estimate. The numerical errors specifically associated with the simulation of diffusion tend to zero as $\nu \to 0$, or as $Re \to \infty$.

Milinazzo and Saffman[23] have criticized Chorin's random vortex method. They model the growth in angular momentum of a continuum vortex by allowing a collection of discrete vortices to undergo a random walk. The variance of the angular momentum is bounded as ν, $t \to 0$, however since ν and t appear in the denominator of their relative error, this error and its variance are infinite in these limits. Milinazzo and Saffman demonstrate that the variance in their relative error can only be contained if the number of elements in the ensemble increases in proportion to the Reynolds number. There is an obvious difficulty in proposing a 'relative error' (which has any significance) for a function which vanishes at one or more points on its domain of definition. Furthermore it seems likely that ensemble averaging (i.e. splitting a computation with a large number of vortices into several computations with fewer vortices) would reduce the expense of this particular computation.

Chorin[24] suggests that a natural expression for the relative error associated with this stochastic simulation would be the difference between the exact expression of angular momentum at time t and its stochastic simulation, divided by the exact expression. Such a relative error is bounded, with zero mean, and with variance which is also bounded, tending to zero as $\nu \to 0$ and as $t \to \infty$.

The manner of expressing the relative error in such a problem is to some extent arbitrary. The whole question of determining criteria for the comparison of continuum processes with their stochastic simulations requires further investigation. At the moment there does not seem to be an established consensus.

3.2. Flow in the presence of boundaries

The error analysis associated with viscous boundary conditions is much less complete than that for unbounded flow. The convergence of Chorin's treatment of the boundary layer is discussed in a general context in Reference 25. His specific model of no-slip and of vortex creation provides convincing simulations of Blasius flow[12] and good agreement with experimental measurements of the drag on cylinders and aerofoils.[14]

The length of each vortex sheet segment is related to the separation distance of the vortices along the boundary; this distance is typically some fraction of the perimeter of the body. Obviously the distance between sheets in the boundary layer will be much smaller than the core dimensions, i.e. the sheets largely overlap. Hald[19] demonstrates for unbounded inviscid flow that the vortex method converges for a core size which can be much larger than the core separation.

Where a boundary separates, Prandtl boundary layer equations are locally no longer a valid approximation. It is difficult to assess the effect to the overall flow of using equation (13) at separation points. The behaviour of vortex segments in this region will be discussed in more detail in the next section.

4. FLOW STARTED IMPULSIVELY AT $t = 0$

An advantage of the method we have described lies in the fact that it can accommodate an inflow velocity field of arbitrary structure. For example, if the velocity profile of the atmospheric boundary layer can be prescribed directly by a power-law formula,

$$\mathbf{u}_f(y) = \mathbf{u}_f(y_g)(y/y_g)^\alpha \tag{18}$$

(with appropriate choice of gradient height y_g and exponent α) then the viscous forces which create this global boundary-layer need not enter explicitly into our model. To treat the case of a building immersed in this atmospheric boundary-layer, we may concentrate on the *perturbation* to $\mathbf{u}_f$ which is generated by the obstacle, i.e. the perturbation field $\mathbf{u}_\xi + \mathbf{u}_\phi$ (and in $\mathscr{B}$ the field $\mathbf{u}_\kappa$). This amounts to: (i) a summation over a finite collection of vortex elements; (ii) a summation over a finite collection of vortex sheets and (iii) an integration over a bounded perimeter in equation (10). Similar to many Green's function methods (and in contrast with many grid methods) there are no boundary conditions to be imposed numerically at infinity.

We shall illustrate the method for the case of an inlet profile described by (18) with $\alpha = 0{\cdot}16$ (a 'rural' profile) around a pitched-roof building for a flow initialized at $t = 0$. Strictly speaking, we consider the viscosity to be 'turned on' at $t = 0$ and hence the viscous effects of the building propagate into a steady free-stream flow. The effects of these starting conditions can be compared to those of an impulsive start-up, with fluid accelerated from rest instantaneously at $t = 0$, to some steady value. Obviously this is an artificial situation and the random vortex method can be extended to treat the physically more realistic case of flow with finite acceleration. In particular, it should be possible to prescribe a continuous transient signature in the time domain for the incident free-stream in order to represent wind gusts. Long period time averages can be computed from the flow which may approach a stationary (or quasi-stationary) state. Since the numerical solution becomes increasingly accurate, in theory converging to an exact solution as the time-interval of each step tends to zero,[26] the method is particularly appropriate for the study of the time-varying aspect of flow in detailed resolution over short periods of time, as opposed to evaluating a steady state. In any case, there are more efficient numerical techniques which can be used to predict a steady flow field around a building (e.g. see Reference 15).

Equation (1) has been expressed in terms of dimensionless variables $\mathbf{u}$, $\mathbf{r}$ and t, which can be converted into dimensional variables by multiplying them by factors U, L and T, respectively: U is a standard scale velocity for the flow, L is scale length and T is given by $T = L/U$. In architectural applications a natural choice for L is the height (or ridge height) of a building, and for U we may choose the free-stream velocity at that height. Typically, $L = 10\,\text{m}$, $U = 5\,\text{m/s}$, and hence $T = 2\,\text{s}$. In the following illustrations, the interval between time-steps is chosen to be 0·02 dimensionless units, and the Reynolds number is 10^6.

The application of image theory in (6) and (9) ensures that there is no convective transport of vortex elements (or of fluid) across the ground plane $y = 0$, however a vortex element may diffuse across this plane into $y < 0$, in which case it is removed from the flow calculation. To limit the computer storage requirements of the calculation, vortex elements are also removed after they have been transported sufficiently far downstream that they no longer influence the flow near the building; in the following examples we take this distance to be fifteen building lengths downstream.

In Figure 2 the random vortex method is illustrated for various buildings with common eaves-height (0·5 dimensionless units) and width (1 unit), but with various angles of roof pitch (0°, 23·5°, 30° and 40°). The extended obstacle is represented by 40 body-points. In each case the building is exposed to an incident wind described by equation (18) with $\alpha = 0{\cdot}16$, and with

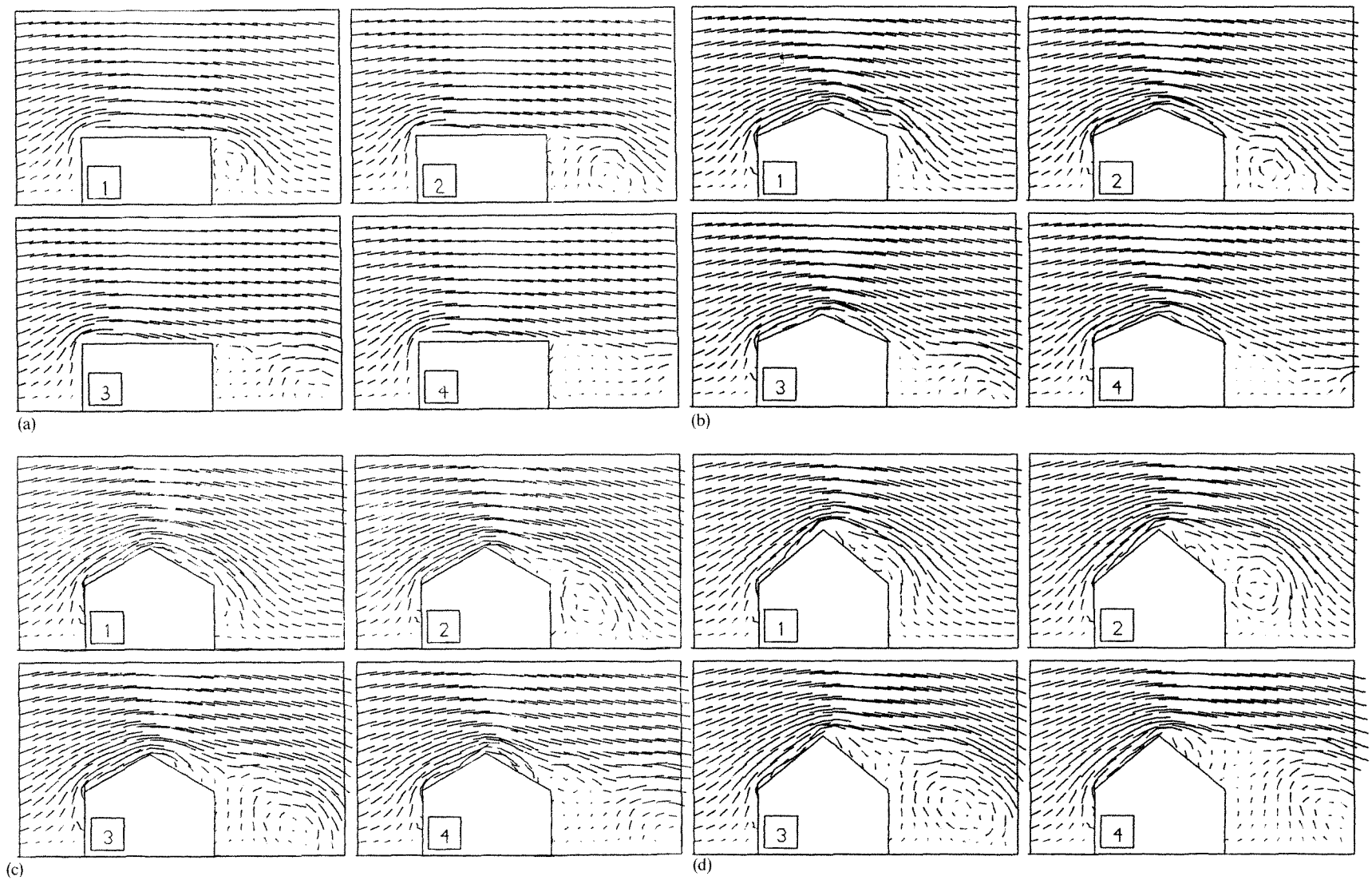

Figure 2. Streaklines illustrating the evolution of flow for (a) a 0° roof pitch; (b) 23·5° pitch; (c) 30° pitch; (d) 40° pitch. The total scaled time interval in each case is 1·5. Each individual streak represents four time-steps

a wind-speed scaled arbitrarily so that u_f at twice the eaves height is taken to be 2·5. For an eaves height of 10 m and a wind speed of 10 m/s at gradient height of 20 m, this would imply a time-scale of $T = 5$ s.

Figure 2(a) illustrates the flow over a block-shaped building. The first frame represents the streak-lines formed by massless particles entered into the flow from a regularly-spaced array of points, at the 18th time-step; the paths of the particles are then followed over four successive time-steps. Since each time-step corresponds to 0·02 dimensionless units of time, at step 21 there have elapsed 0·42 dimensionless units of time since the impulsive start-up. At the 21st time-step there are 253 discrete vortex elements and segments entered into the flow. The second frame of Figure 2(a) represents the flow between time-steps 36 and 39 (with 352 elements in the flow); the third frame represents flow between time-steps 54 and 57 (378 elements); the fourth frame represents steps 72 to 75 (446 elements). The entire sequence represents 1·5 dimensionless units of time, or 7·5 s if $T = 5$ s.

Various aspects of the flow development in its initial stages can be visualized in Figure 2(a): at the windward eaves there develops a sharp separation with some suggestion of reattachment onto the horizontal surface of the roof. (Castro[4,6] discusses some experimental evidence to suggest such reattachment.) At the leeward eaves a recirculation eddy forms which detaches and then begins to convect downstream.

Figure 2(b) illustrates the initial flow development over the same intervals of time, but for the case of building with roof pitch 23·5°. At the 75th time-step there are 607 vortex elements entered in the flow. Figure 2(c) illustrates the development of flow for a roof-pitch of 30° (at the 75th time-step there are 556 vortex elements in the flow). Figure 2(d) illustrates the initial flow development for roof-pitch of 40° (at time-step 75 there are 571 elements in the flow).

A comparison of Figures 2(a)–2(d) indicates the effect of roof geometry on the pattern of initial flow development. The separation at the windward eaves moves to the ridge as pitch is increased, and reattachment can occur on the leeward roof. In the initial stages, a recirculation eddy appears to form along the leeward roof, before it detaches itself and convects downstream. This latter feature resembles flow visualizations from some well-known water-channel experiments (see plate 9 in Reference 27).

The streakline diagram (Figure 3(a)) illustrates the sequence of flow development (for 40° roof pitch) after a total of 220 time-steps have elapsed. This represents a dimensionless time interval of 4·4, or some 22 s if $T = 5$ s. Figure 3(b) illustrates the locations (and sense) of the corresponding 805 discrete vortex elements in the flow. It can be seen from Figure 3 that a wake is developing, which appears to 'reattach' downstream of the building, although as time progresses further, this position varies considerably. Wilson *et al.*[7] have compiled a comparison of published experimentally-determined cavity lengths and flow reattachment lengths behind various obstacles mounted in a boundary-layer; these lengths vary from 4 building lengths to some 16 building lengths downstream, depending on Reynolds number, boundary-layer thickness, and obstacle shape. In their own water channel and wind tunnel experiments, they studied the effect of Reynolds number on the reattachment length behind a hill-model, characterized by an apex angle of some 20°. They found that the reattachment length becomes shorter with increasing Reynolds number: for a flow Reynolds number varying between 10^2 and 10^4 this length varies between 6 and 4 times the hill-height.

Experiments such as these indicate that a large-scale recirculation bubble can achieve considerable stability in the wake. (This is also a prominent feature of steady numerical solutions to the Navier–Stokes equation for high Reynolds number.) However, the present simulation does not render this stationary flow feature. It may be that a stationary recirculation bubble is to be associated with longer time-averages. Alternatively, an inspection of Figures 3 and 4 might suggest

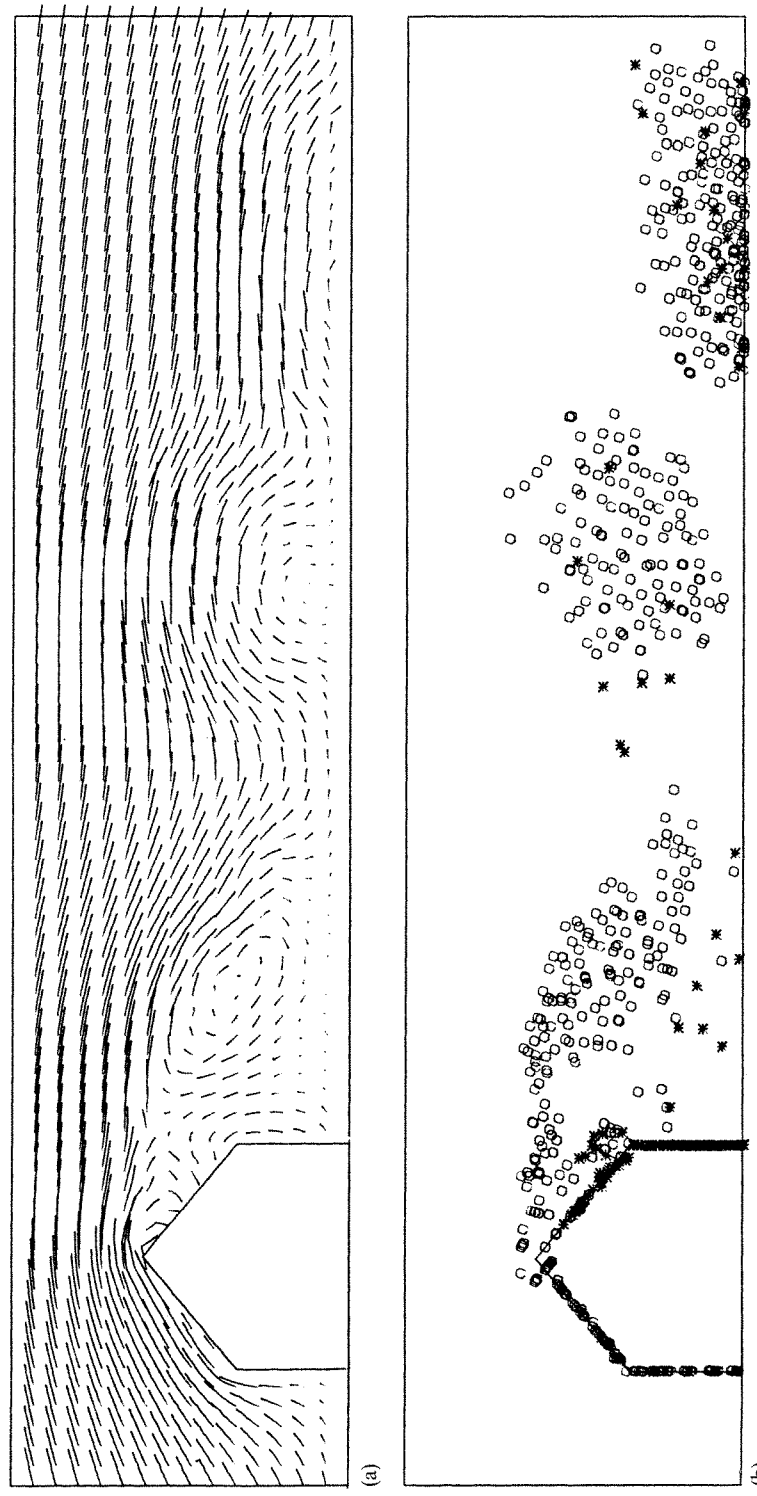

Figure 3 (a) Streaklines evaluated after a scaled time interval of 4·4 has elapsed; (b) the locations of discrete vortex elements in the flow (○ represents positive vorticity, * negative vorticity)

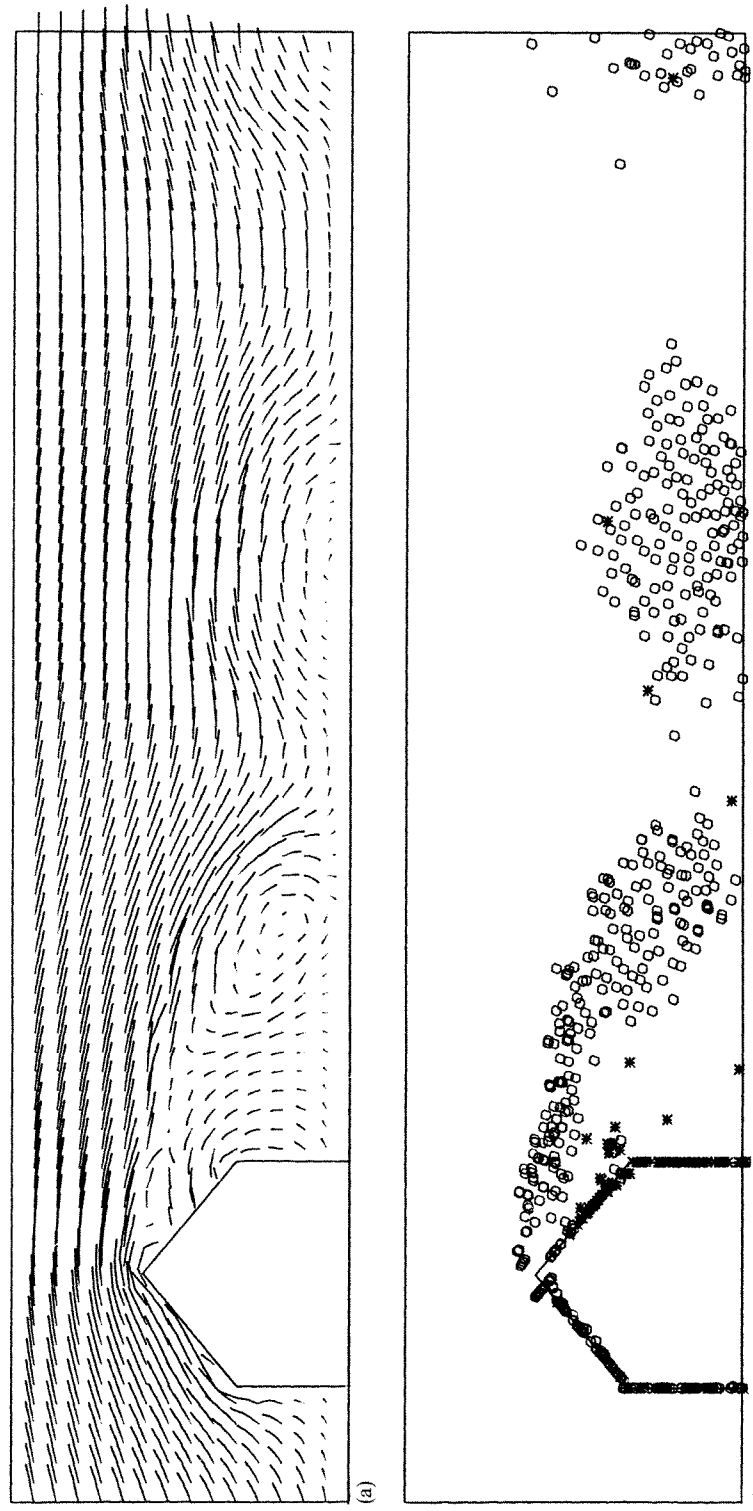

Figure 4. Streaklines and vortex locations after a scaled time interval of 6 units

that a viscous interaction of the ground with the cluster of vortices after they have detached from the roof could be a significant factor in determining the character of the wake. Downstream from the obstacle, the no-slip condition has not been imposed at the ground plane, so detached eddies are able to slip freely downstream. A more comprehensive model could be constructed by introducing body-points along the plane $y = 0$. In the present simulation the evolution of a recirculation bubble is not pursued, and we concentrate on the obstacle itself during the initial stages of vortex shedding.

The shapes of the first two clusters of discrete vortices which have detached in Figure 3(b) are anomalous and can be associated with the initial conditions whereas subsequent clusters assume a more regular and distinctive shape. A more regular sequence is illustrated in Figure 4 for flow at a scaled time of 6 dimensionless units. Despite their increasing regularity of shape, as time progresses further, the frequency with which the large lee eddies detach at the body appears to remain unsteady. Some frequency-spread in the spectrum is anticipated by wind-tunnel experiment for the streamwise shedding from a surface-mounted obstacle: the measured periodicity content of a fully developed wake is not sharply-defined (e.g. see Figure 13 in Reference 6), unlike the case of spanwise shedding which establishes a vortex street (see Figures 15 and 16 in Reference 3).

As we have already noted, at the apex of the obstacle where the flow separates, vortex sheet segments are subject to large velocities vertical to the building surface. The elements which penetrate into the building (beyond $y' < \partial\mathscr{B}'$) are removed from the calculation. Those which

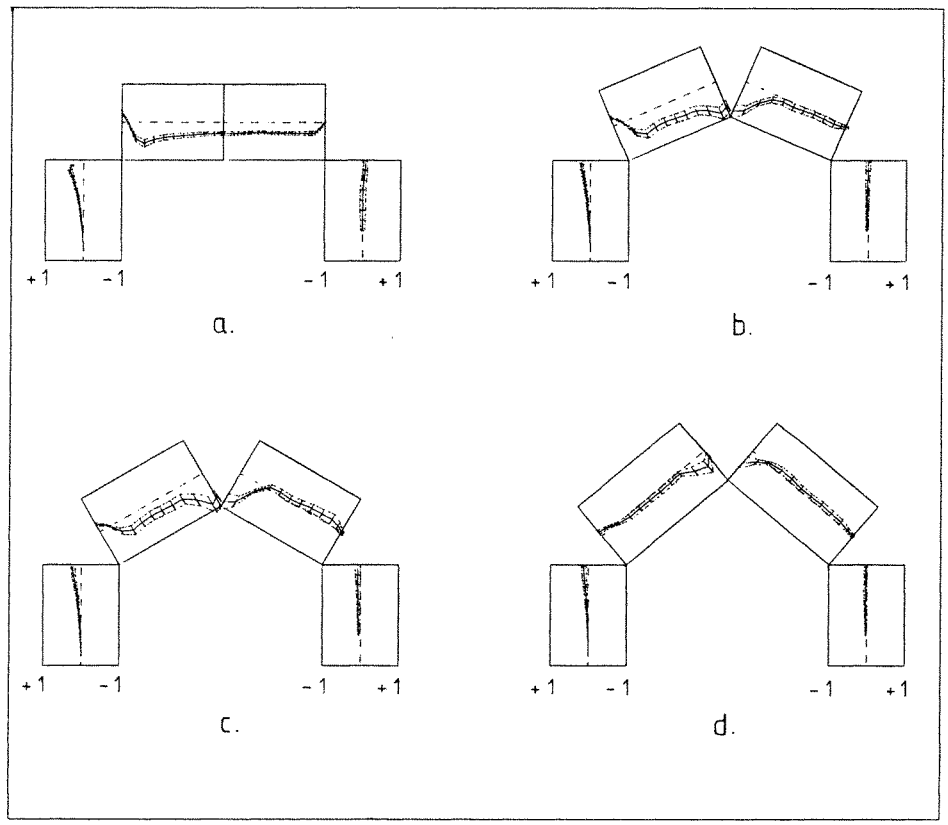

Figure 5. Distribution of computed C_p averaged over 75 time-steps, derived from the velocity fields illustrated in Figure 2. The dotted envelope represents the standard deviations associated with C_p

move into $\mathscr{C}$ are then subject to Navier–Stokes flow. This behaviour indicates large gradients in the velocity field in $\mathscr{B}$ near the apex (possibly associated with the accumulation of vortex segments which have convected from $\mathscr{B}$ 'upstream' of the apex). These velocity gradients are not consistent with the Prandtl equations, and separation represents a point of particular inaccuracy in the method. A detailed study of the vorticity dynamics in the vicinity of separation is required to assess the errors there.

It is nevertheless interesting that this behaviour of vortex segments near points of separation is reminiscent of the practice used in a number of vortex methods whereby discrete vortices are injected into flow at determined points of separation.[28–30] This process appears to arise in Chorin's method as a natural consequence of the no-slip condition.

5. A NUMERICAL DETERMINATION OF PRESSURE COEFFICIENT

If the velocity field $\mathbf{u}(x, y, t)$ has been determined numerically, and in sufficient geometric detail, then in principle the pressure field can be calculated from it. Specifically, if the first- and second-order partial derivatives of $\mathbf{u}$ can be numerically computed then ∇p can be determined from the Navier–Stokes equation. Once this pressure gradient is known, then by integration the pressure itself can be derived anywhere in the flow—so long as this pressure can be independently fixed at some single reference point in the flow. For this purpose we shall choose a point $(x_{\text{ref}}, y_{\text{ref}})$ upstream to which a stagnation pressure p_{ref} can be attached. We note too that it is our purpose to normalize (through the calculation of a pressure coefficient) all computed pressures with respect to this value p_{ref}. From the point of view of the present calculation this may be set arbitrarily to unity, i.e.

$$p_{\text{ref}} = \tfrac{1}{2}\rho u_{\text{ref}}^2 = 1.$$

All subsequent pressure calculations must hence be considered to be normalized with respect to $\frac{1}{2}\rho u_{\text{ref}}^2$.

To relate the mean pressure at a point on the building to the reference pressure p_{ref}, a point y_{ref} is chosen to be at building height (or at eaves height in the case of a pitched-roof building), such that $y_{\text{ref}} = y_e$, so that the x-component of the Navier–Stokes equation can be used to relate pressure p_e on the windward side of the building at (x_e, y_e) to the upstream stagnation pressure p_{ref}. The left-hand side of

$$\frac{\mathrm{d}p}{\mathrm{d}x} = \frac{1}{Re}\left\{\frac{\partial^2 u}{\partial x^2} + \frac{\partial^2 u}{\partial y^2}\right\} - \left\{u\frac{\partial u}{\partial x} + v\frac{\partial u}{\partial y}\right\}, \tag{19}$$

is integrated over the domain from x_{ref} to x_e. We have here neglected the transient term in the Navier–Stokes equation since we are concerned to establish a relative mean pressure on the building. The numerical problem can be approached by a finite-difference analogue to (19), evaluating the derivatives on its right-hand side by difference formulae accurate to second-order. At the building surface we take a one-sided second-order formula.

Having determined the (normalized) mean pressure p_e at a point (x_e, y_e) on the windward face of the building, we can now evaluate the pressure distribution relative to this pressure along the building surface. Since the condition of no-slip is satisfied along this surface, the pressure gradients assume the simplified expressions:

$$\begin{aligned}\frac{\mathrm{d}p}{\mathrm{d}x} &= \frac{1}{Re}\left\{\frac{\partial^2 u}{\partial x^2} + \frac{\partial^2 u}{\partial y^2}\right\},\\ \frac{\mathrm{d}p}{\mathrm{d}y} &= \frac{1}{Re}\left\{\frac{\partial^2 v}{\partial x^2} + \frac{\partial^2 v}{\partial y^2}\right\}.\end{aligned} \tag{20}$$

These gradients can be expressed, after simple rotation, in components aligned parallel to, and perpendicular to, the building surface. With the numerically determined function dp/ds known along the perimeter of the building (with tangential unit vector **s** defined as before), we can perform a numerical integration of this tangential gradient, using for example a trapezoidal rule. The integration is performed over $\partial\mathscr{A}$ in such a way that p is continuous along the surface and $p(x_e, y_e) = p_e$ at the point of reference on the building (this latter condition essentially specifies the overall constant of integration). At discontinuities in the geometry of the surface, dp/ds is not properly defined, so some precaution must be taken to ensure that median values of (**s**, **n**) are chosen at these points. Inevitably this contributes an additional error in the estimation of pressure at the building's corners. In this context it should also be noted that the accuracy with which equation (10) can be solved numerically is adversely affected by discontinuities in $\partial\mathscr{A}$, since such corners are excessively smoothed by the numerical procedure. (The matrix equation is well conditioned, however, and the procedure is stable.) The accuracy can be improved by approximating re-entrant corners as minutely 'bevelled'.

To express the pressure distribution over the surface of the building in terms of the pressure coefficient, C_p, the integration is performed in such a way that $p(x_e, y_e) = p_e - p_{ref}$. The engineering significance of this coefficient is discussed in References 31, 32 and others.

Figure 5 illustrates the distribution of pressure coefficients over the same building forms shown in Figure 2. The pressure is averaged over an interval of 75 time-steps; the standard deviation is indicated by the envelope of dotted lines. Negative values of C_p indicate suction. The curves of Figure 5 show some qualitative similarity with wind-tunnel measurement, but the leeward suction indicated by the simulation is less pronounced than most measured values. It will be observed that for the 0° pitch case, a slight positive pressure appears at the lee corner, and this tends to broaden and move towards the apex as pitch angle is increased. The question of the leeward pressure is discussed further in the next section.

6. COMPARISON WITH WIND-TUNNEL EXPERIMENT

Some indication of the plausibility of the random vortex simulation can be found in a comparison with wind-tunnel measurements. For example, Castro[4] provides a detailed description of experiments to determine the flow over two-dimensional square section blocks mounted in a thick rough wall boundary layer. His experiment is primarily concerned to examine the wake downstream of reattachment; his Figure 6 displays various distributions of pressure coefficient over the block perimeter.

Before comparing the present numerical simulation to such wind-tunnel data, some important cautionary notes must be sounded. In the present simulation a sheared *stationary* inlet flow is prescribed, whereas the rough wall boundary layer of Castro's experiment possesses a measured turbulence structure. In a wind-tunnel experiment, the mean estimates of pressure at the block surface are taken experimentally over extended averaging periods with stationary or quasi-stationary conditions for the wake. In the present numerical simulation we confine ourselves to rather short time averages (at most over 3 units of scaled time after flow initialization), during which a stationary recirculation bubble has not developed.

The block surface pressures measured by Castro (Reference 4, Fig. 6) display an interesting contrast between two sets of flow conditions (these are tabulated by Castro in his Tables 1 and 2). Two flows (designated 'F1L' and 'F1S') are both associated with a boundary-layer which can be described by a power-law profile (18) with exponent $\alpha = 0{\cdot}19$. The square section obstacle for the flow 'F1L' is nominally of height 65 mm, and for the flow 'F1S', of height 12 mm. The parameters required to effect our numerical simulation are tabulated in Table I where the Reynolds number, Re, is based on free-stream velocity and block height, H.

Table I

	Re	$u_f(H)/u_f(\infty)$	α
'F1L'	15,000	0·685	0·19
'F1S'	7500	0·58	0·19

Using the flow parameters of Table I, we have tried to simulate this flow (excluding, as we have explained, the effect of upstream turbulence). Figure 6 illustrates the distribution of simulated C_p determined for these two cases, and these are compared to Castro's measurements. The extended block geometry is represented by seventy-two body-points. The numerical simulation consists of an average over 100 time-steps after flow initialization, each time-step of duration 0·025 scaled units. The standard deviation associated with this mean is also indicated in Figure 6.

In view of the differences between the numerical model and the conditions of Castro's experiment, it is interesting to see the degree of similarity between these pressure distributions. The discrepancy between them can also be noted. Particularly at the lee side of the block, our numerical simulation does not reproduce the strong rather uniform suction measured by Castro. It may be the case that the present numerical model is not adequate to determine this suction, since we have confined ourselves to a short-interval average and we do not have a stationary recirculating wake. It can also be noted that the suction over the top of the block in the numerical simulation is less

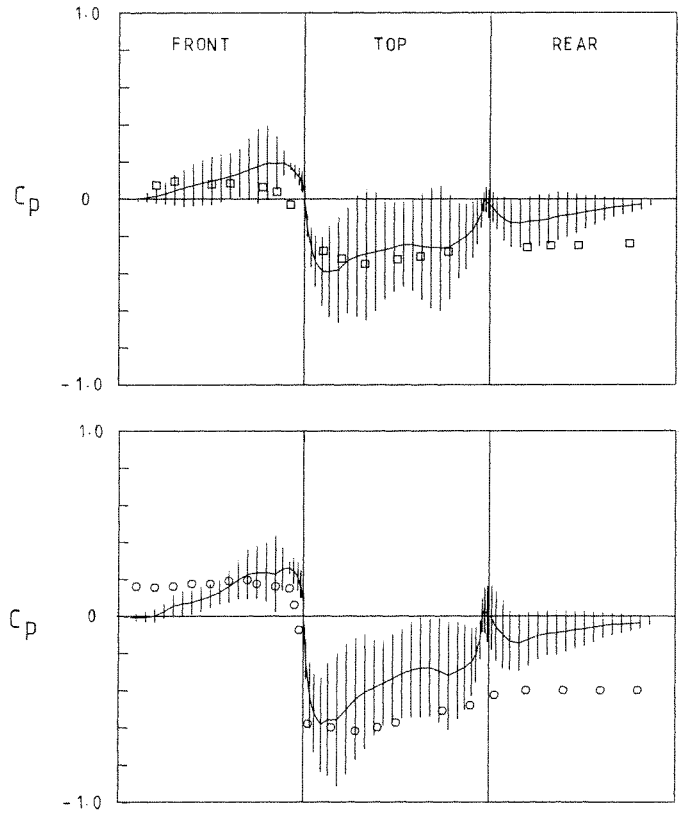

Figure 6. Comparison of computed C_p (solid line with standard deviation bars) with the measurements of Castro (Reference 4, Figure 6)—□ for flow 'F1S', and ○ for flow 'F1L' (parameters in Table I)

than the measured values: this may be again related to the shortness of the averaging interval, or to the absence of vorticity in the incident stream. Lee[3] demonstrates that an increase of incident turbulence has the effect of raising base surface pressure. This suggests that introducing turbulent inlet conditions could increase the suction on the building.

Castro's Figure 6 indicates a magnitude of C_p for 'F1L' on the windward face which is roughly twice that for 'F1S', and it will be noted that this is similar to the ratio of the Reynolds numbers for the two cases. It would be valuable to know how the pressure distribution over an obstacle varies with varying Reynolds number. Of course, at low Reynolds number the viscous term in the Navier–Stokes equation has an important influence on the pressure field near a solid boundary; the situation at high Reynolds number is less clear. It is a widely held view that C_p is not measureably dependent on Reynolds number for $Re > 5000$, and this forms a basis for the application of scale model studies to large-scale flow problems. In view of the inviscid character of the error in the present simulation, it should be possible to examine any dependence of C_p on Reynolds number.

To illustrate this, the numerical computations associated with Figure 6 are simply repeated for the same Reynolds numbers, however the velocity at block height is now chosen to be the same in both cases. A scaled velocity of 0·87 is chosen (corresponding to a velocity of unity at a gradient height of $2H$ for $\alpha = 0{\cdot}19$). The two curves in Figure 7 should reflect solely the difference in Re for the two cases. It can be observed that the pressures on the windward face are very similar for the two cases; over the top of the block the two pressure distributions differ. The computed C_p at the

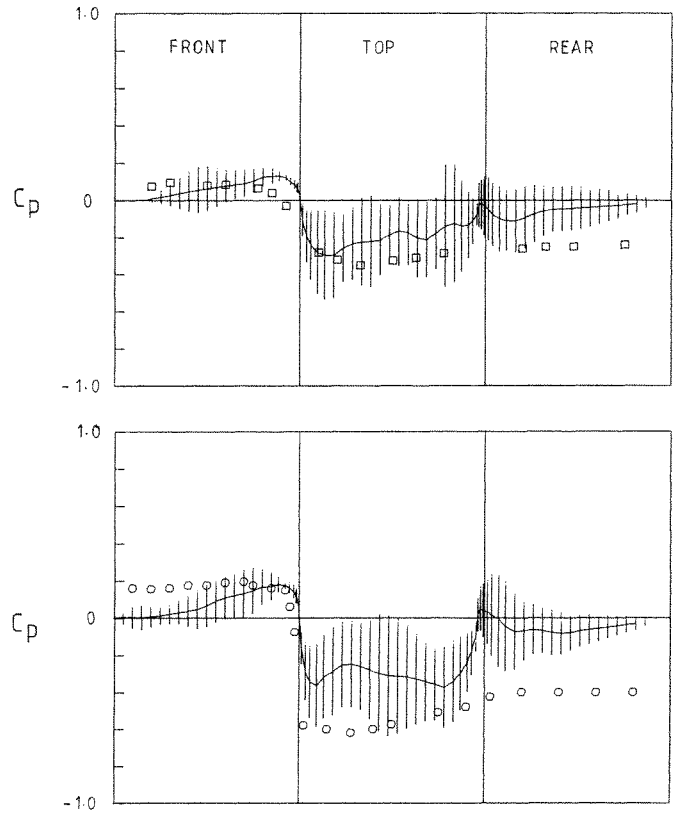

Figure 7. Comparison of computed C_p for two Reynolds numbers $Re = 7500$ (upper diagram) and $Re = 15{,}000$ (lower diagram). The free-stream velocity at block height is 0·87 in both cases

windward face suggests that the measured differences in C_p between 'F1L' and 'F1S' are more related to block-height velocity than to Reynolds number. The two curves in Figure 7 represent a mean over a short averaging interval (2·5 dimensionless units) and this mean has not yet achieved a steady value. Thus the differences between the two curves of Figure 7 cannot be offered as conclusive evidence of a dependence of C_p on Reynolds number; further numerical experiment would be required. In any case Figure 7 does serve to illustrate how numerical experiment might be applied to the question and a comparison between Figures 6 and 7 will indicate how an increase in the block-height free-stream velocity (normalized with respect to the free-stream) can influence the simulated pressure averaged over the same scaled time interval.

Finally we show the application of the method to a structure with a pitched roof. Holmes and Best[33] have made measurements in a boundary layer wind-tunnel (for a rural profile) over a low-rise three-dimensional building form with 10° pitch gable roof with overhanging eaves. The model has a ratio of cross-section width to axial length to eaves height of 7:14:3. The measurements were made over its perimeter in cross-section along a band of pressure panels on the centre-line of the model building. The width-to-height aspect ratio is certainly not sufficiently large to exclude three-dimensional effects, nevertheless Figure 8 does show that the random vortex method provides a centre-line pressure distribution similar to the measured values in Reference 33, Table 1. In view of the differences between a two-dimensional and a three-dimensional flow, this similarity may be fortuitous.

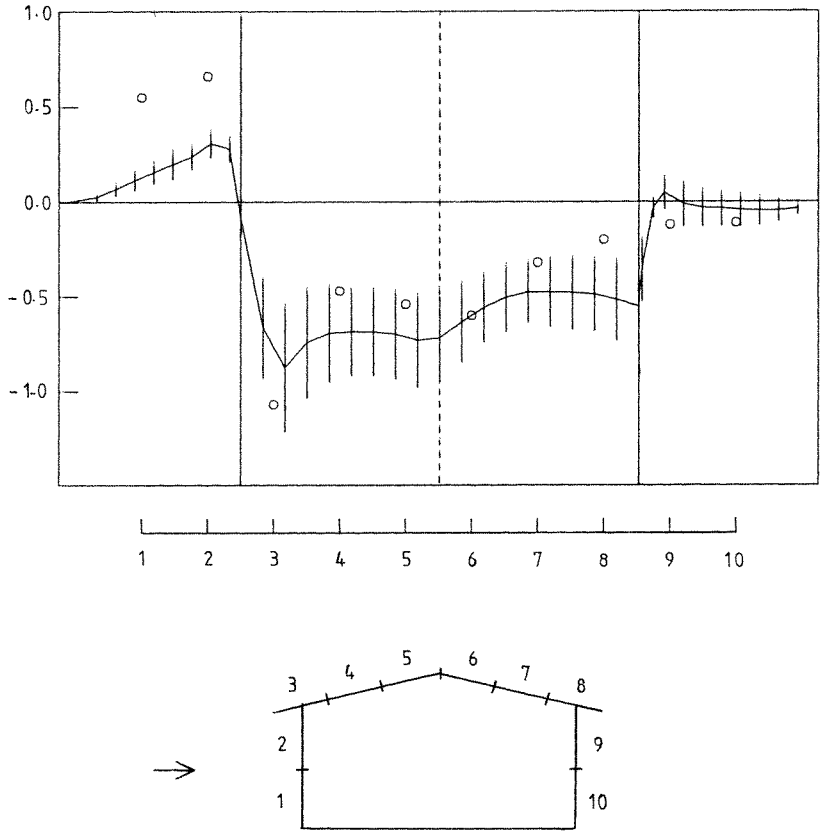

Figure 8. Comparison of computed C_p (solid line) with the measurements (open circles) of Holmes and Best (Reference 3, Table 1)

The two-dimensional numerical model associated with Figure 8 consists of a building form with 10° roof pitch and a scaled width of 1; width-to-height ratio is 7:3; an inlet profile is of power $\alpha = 0{\cdot}16$; the Reynolds number is 10^4 (corresponding to typical wind-tunnel conditions). The velocity at eaves-height is 1 dimensionless unit. The pressure coefficient is averaged over 100 time-steps each of duration 0·02 dimensionless units. The standard deviation of this computed C_p is indicated by the bars.

The large pressures measured by Holmes and Best at the panels on the windward face may be explained by the substantial roof overhang which we have not modelled in our simulation (although it is possible to model such a feature).

7. CONCLUSIONS

The random vortex method can be used to study, by means of numerical experiment, the mechanics of wind-flow over buildings. The dynamic evolution of flow can be simulated, including the case of wind-flow which is impulsively started; high frequency fluctuations in the flow can also be modelled. The method does not generate numerical dissipation and hence it can depict the influence of Reynolds number on the pattern of flow. Unlike a number of other vortex methods, the method of Chorin does not require *a priori* knowledge of flow separation points. For two-dimensional problems, the geometrical shape and disposition of obstacles in the flow is arbitrary; the influence on a building of its neighbourhood can be modelled. The form of the free-stream field, $\mathbf{u}_f$, is also arbitrary; as we have shown, this may be chosen to simulate a power-law boundary layer profile.

It should be possible to simulate specific conditions of incident wind-turbulence by artificially introducing point sources of (discrete) vorticity upstream. Alternatively, upstream surface roughness can be introduced and the vorticity-creation algorithm itself can be used to generate 'turbulence' in the incident stream.

Some comparisons have been made with wind-tunnel measurements, but these are preliminary and cannot be taken as a benchmarking exercise. More detailed consideration would need to be taken of the relationship between experimental and numerical conditions. Furthermore, the effect of the wake development would need to be studied numerically.

A number of obvious improvements to the present implementation can be suggested. The geometrical definition of the obstacle can be improved by increasing its number of 'body-points': this is of particular importance if the modelling of sharp features (such as eaves) is to be contemplated. If the evolution of a stable (or at least quasi-stationary) recirculating wake is to be studied, then some attempt must be made to introduce a thin plate of body points at the ground level downstream from the obstacle. Such a model would be necessary if adequate comparison is to be made with data derived from quasi-stationary experimental conditions. Perhaps upstream boundary-layer separation should also be modelled in order to determine how this contributes to the wind interaction with a building.

The random vortex method can be easily adapted to study a number of particular structural and environmental problems. It is possible to model the effect of small-scale structural elements such as eaves. Also the airborne dispersion of effluent and the flow of wind over topographical features can, in principle, be modelled. More fundamentally, the method could be used to assist in investigating the physical mechanisms of flow separation, vortex shedding and wake formation. Some authors (e.g. Reference 2) have formulated a simple theory to relate the shedding and reattachment dynamics of flow over a surface-mounted obstacle to the parameters of upstream turbulence. The simulations described in the present paper re-enforce the observed fact that *non-periodic* inlet conditions can lead to surface pressure fluctuations, shedding and wake formation solely through

the viscous interaction of the flow field with the obstacle. Perhaps it may be appropriate to consider more carefully such shedding phenomena primarily as a physical consequence of the no-slip condition. Of course, such an emphasis must not detract from the importance of upstream conditions.

The random vortex method has been extended to three-dimensions[13,20] in various other aerodynamic contexts; for the problem of flow over arbitrarily-shaped surface-mounted obstacles, a three-dimensional formulation of the problem would involve a considerable increase in geometrical complexity.

The computer storage requirements for the calculations illustrated in this paper are modest. The numerical solution illustrated in Figure 2(a) required 640s cpu and 210 K bytes of storage (on a DEC System-10); however run time can escalate as more discrete vortices enter the flow in order to achieve longer time averages. (For example, a run over the time interval between time-steps 300 and 380, with between 800 and 900 discrete vortices entered in the flow, requires 3780 s cpu.) Obviously any increase in the resolution of body-definition or in time-resolution, or any attempt to model a three-dimensional obstacle, would necessitate increased computer requirements. It is interesting to note that the random vortex algorithm lends itself to implementation on a distributed array processor (such as the ICL-DAP); such implementation could make accessible more ambitious modelling problems than those presented in this paper.

ACKNOWLEDGEMENTS

This work was supported by the U.K. Science and Engineering Research Council under grants GR/A/8632.9 and GR/B/9220.1. The authors than K Prof. A. J. Chorin for his interest in this work.

REFERENCES

1. A. J. Chorin, 'Numerical study of slightly viscous flow', *J. Fluid Mech.*, **57,** 785–796 (1973).
2. J. Counihan, J. C. R. Hunt and P. S. Jackson, 'Wakes behind two-dimensional surface obstacles in turbulent boundary layers', *J. Fluid Mech.*, **64,** 529–563 (1974).
3. B. E. Lee, 'The effect of turbulence on the surface pressure field of a square prism', *J. Fluid Mech.*, **69,** 263–282 (1975).
4. I. P. Castro, 'Relaxing wakes behind surface-mounted obstacles in rough wall boundary layers', *J. Fluid Mech.*, **93,** 631–659 (1979).
5. I. Grant and F. H. Barnes, 'The vortex shedding and drag associated with structural elements', *J. Wind Eng. Ind. Aerodyn.*, **8,** 115–122 (1981).
6. I. P. Castro, 'Measurements in shear layers separating from surface-mounted bluff bodies', *J. Wind Eng. Ind. Aerodyn.*, **7,** 253–272 (1981).
7. D. J. Wilson, G. Winkel and O. Neiman, 'Reynolds number effects on flow recirculation behind two-dimensional obstacles in a turbulent boundary layer', *Proc. 5th Int. Conf. Wind Eng.*, Pergamon Press, Oxford, 1980.
8. D. M. Deaves and R. I. Harris, 'A mathematical model of the structure of strong winds', *CIRIA Report 76*, London, 1978.
9. B. E. Lee, 'An investigation of the effects of turbulence scale on the mean forces on two-dimensional square prisms', Department of Building Science, University of Sheffield, *Report BS24*, 1975.
10. K. J. Eaton, J. R. Mayne and N. J. Cook, 'Wind-loads on low-rise buildings—effects of roof geometry', *BRE Current paper CP1/76*, Garston, U.K. 1976.
11. C. W. Newberry, 'Significant features of wind loading in relation to the design of structures', *BRE Current paper CP49/69*, Garston, U.K., 1969.
12. A. J. Chorin, 'Vortex sheet approximation of boundary layers', *J. Comput. Phys.*, **27,** 428–442 (1978).
13. A. J. Chorin, 'Vortex models and boundary layer instability', *SIAM J. Sci. Stat. Comput.*, **1,** 1–21 (1980).
14. A. Y. L. Cheer, 'Numerical study of incompressible slightly viscous flow past blunt bodies and airfoils', *SIAM J. Sci. Stat. Comput.*, **4,** 685–705 (1983).
15. T. Hanson, D. M. Summers and C. B. Wilson, 'Numerical modelling of wind flow over buildings in two-dimensions', *Int. j. numer. methods fluids*, **4,** 25–41 (1984).
16. A. F. Ghoniem, A. J. Chorin and A. K. Oppenheim, 'Numerical modelling of turbulent flow in a combustion tunnel', *Phil. Trans. R. Soc. Lond.*, **A304,** 303–325 (1982).
17. L. E. Fraenkel, 'On corner eddies in plane inviscid shear flow', *J. Fluid Mech.*, **11,** 400–406 (1961).
18. P. J. Roache, 'On artificial viscosity', *J. Comput. Phys.*, **10,** 351–366 (1972).

19. O. H. Hald, 'Convergence of vortex methods for Euler's equations II', *SIAM J. Numer. Anal.*, **16,** 726–755 (1979).
20. A. Leonard, 'Vortex methods for flow simulation', *J. Comput. Phys.*, **37,** 289–335 (1980).
21. J. Marsden and A. Weinstein, 'Coadjoint orbits, vortices, and Clebsch variables for incompressible fluids', *Physica D*, in press.
22. J. T. Beale and A. Majda, 'Rates of convergence for viscous splitting of the Navier–Stokes equations', *Math. Comp.*, **37,** 243–259 (1981).
23. F. Milinazzo and P. G. Saffman, 'The calculation of large Reynolds number two-dimensional flow using discrete vortices with random walk', *J. Comput. Phys.*, **23,** 380–392 (1977).
24. A. J. Chorin, 'A comment on the paper "The calculation of large Reynolds number flow using discrete vortices with random walk" by F. Milinazzo and P. G. Saffman', *J. Comput. Phys.*, **26,** 453–454 (1978).
25. A. J. Chorin, T. Hughes, M. McCracken and J. E. Marsden, 'Product formulas and numerical algorithms', *Comm. Pure and Appl. Math.*, **31,** 205–256 (1978).
26. J. Marsden, 'A formula for the solution of the Navier–Stokes equations based on a method of Chorin', *Bull. Amer. Math. Soc.*, **80,** 154–158 (1974).
27. G. K. Batchelor, *An Introduction to Fluid Dynamics*, Cambridge University Press, Cambridge, 1967.
28. R. R. Clements, 'An inviscid model of two-dimensional vortex shedding', *J. Fluid Mech.*, **57,** 321–336 (1973).
29. T. Sarpkaya, 'An inviscid model of two-dimensional vortex shedding for transient and asymptotically steady separated flow over an inclined plate', *J. Fluid Mech.*, **68,** 109 (1975).
30. R. I. Lewis, 'Surface vorticity modelling of separated flows from two-dimensional bluff bodies of arbitrary shape', *J. Mech. Eng. Sci.*, **23,** 1–12 (1981).
31. A. J. Macdonald, *Wind loading on Buildings*, Applied Science Press, London, 1975.
32. T. V. Lawson, *Wind Effects on Buildings*, Applied Science Press, London, 1980.
33. J. D. Holmes and R. J. Best, 'An approach to the determination of wind load effects on low-rise buildings', *J. Wind Eng. Ind. Aerodyn.*, **7,** 273–287 (1981).